Characterizing The CH₃SSCH₃-Au(111) System From Single Molecules To Full Surface Coverage — A Scanning Tunneling Microscopy Study.

Yi C. Zhang, † David Y. Lee, ‡ K. W. Hipps†

[†]Materials Science & Engineering Program and Department of Chemistry, Washington State University, Pullman, Washington 99164, United States

[‡]INFICON, East Syracuse, New York 13057, United States

Abstract: The adsorption process of dimethyl disulfide onto the Au (111) surface was resolved with subnanometer resolution at temperatures below 130K. We report two temperature dependent adsorption studies to reach totally different surface morphologies for this CH₃SSCH₃-Au(111) system. Starting with a cold-synthesis approach at low-temperature and low coverage the STM images reveal preferential adsorption at specific regions on the Au(111) herringbone reconstructed surface. However, at saturated surface coverage, annealing at 80K leads to self-assembly of an epitaxial monolayer of CH₃SSCH₃ that is influenced by the anisotropic nature of the herringbone reconstruction. In contrast, depositing CH₃SSCH₃ at 80K and above leads to simultaneous adsorption of CH₃SSCH₃ and dissociated SCH₃ fragments on the surface. Saturation coverage of CH₃SSCH₃ deposited on an 80K Au surfaces produces no self-assembled monolayer. DFT calculations are used to provide insights into these two synthesis methods that lead to a discrepancy in surface morphology in the CH₃SSCH₃-Au(111) system. We also demonstrate both tip induced and UV induced dissociation of CH₃SSCH₃ at cryogenic temperatures. We find that the spatial distribution of the UV produced fragments is significantly greater than that of those produced by tip electrons indicating differing mechanisms for the two processes.

Introduction. Supramolecular systems comprised of organosulfer molecules on metal surfaces have drawn significant attention in the fields of catalysis, molecular electronics, and nonlinear optical materials. 1- 10 Common sulfurbased molecules used for particular surface functionalization include alkyl thiols, disulfides, and aromatic thiols. 11-15 In addition to their ability to self-organize on a metal surface, these systems shows great promise in the future of nanotechnology. 16-20 Specific metal surfaces such as Au(111) are common in surface studies due to its ease of manufacturing, availability, and most importantly resistance to chemical activity.21 The nature of the Au(111) surface reconstructs into the 22×V3 herringbone structure due to the introduction of additional atoms in the first atomic layer. The additional gold atoms are inserted into the $\langle 1\overline{1}0\rangle$ crystallographic direction and create an anisotropic surface. This anisotropy leads to periodic variation of the first atomic layer of gold which gives rise to different fcc and hcp domains separated by soliton lines. 22 Besides sulfur-based molecules, several studies on the adsorption and self-assembly of small aromatic compounds are also known to be influenced by the herringbone reconstruction. $^{23-25}$

Using a low-temperature scanning tunneling microscope (LT-STM) under ultra-high vacuum (UHV) condition, we examined different adsorption processes of dimethyl disulfide

(DMDS), CH₃SSCH₃, deposited onto the reconstructed Au(111). This system shows process dependent discrepancies in the final morphologies. surface Two contrasting approaches were adopted: (1) a cold-synthesis approach by depositing DMDS on a cold (12K) surface followed by annealing at a higher temperature; and (2) a hot-synthesis approach by depositing DMDS at two elevated temperatures of 80K and 120K. Each approach was characterized in detail by STM in a range of surface coverages ranging from isolated molecule to surface saturation. Furthermore, we employed density-functional-theory (DFT) to supplement our analysis of the STM data for this DMDS-Au(111) system. Based on the STM images, DMDS shows different adsorption different surface behavior resulting in morphologies depending upon the deposition thermal history. We attribute the differences in surface morphologies to dissociation of some of the DMDS. This is in contrast to a previous report in the literature suggesting that DMDS adsorbs non-dissociatively on Au(111) at temperatures less than 150K.²⁶

II. Experimental Details. Epitaxial gold, Au(111) thin films with thickness 1800-2000 Å were grown on mica, in-house, with a cryo-pumped chamber at a working pressure less than 1.0×10⁻⁹ Torr. The thin films were transferred to the UHV chamber before being annealed in vacuum with base pressure less than 3.0×10⁻¹⁰ Torr. Prior to the exposure to DMDS, surface quality of the Au(111) substrate were examined by STM to reveal well-defined terraces, singleatomic steps and reconstruction line spacing ranging from 63 to 90 Å. The main equipment of the system is a low-temperature UHV STM (model PanScan Freedom) and a controller (model R9+) purchased from RHK technologies. All STM images were acquired at 12K, in constant current mode with a bias voltage of 400-500 mV and a current set point of 10-50 pA. The STM tips are made from chemically etching 0.25 mm diameter Pt_{80}/Ir_{20} wires.

Dimethyl disulfide with purity greater than 99.0% (purchased from Sigma Aldrich) was degassed using several freeze-pump-thaw cycles prior to UHV deposition. The high-purity DMDS chemical was then introduced into the UHV chamber by a leak valve with its nozzle directly aligned to the sample surface at a rate of approximately 2.0×10^{13} molecules/second. Depending on the experimental conditions, the leak valve is opened between 3 – 25 seconds at the specified rate. A Model 325 Cryogenic Temperature Controller (by Lake Shore Cryotronics) is used to control and monitor the sample temperature during and after the DMDS exposure. Deposition temperatures in this study are set at 12K, 80K, and 120K.

Single-molecule dissociation of DMDS was conducted via two methods: (1) STM tip produced current pulses following a previously reported method^{27,28} and (2) UV photon irradiation. The tip pulse conditions were set at a 100 ms pulse duration at 1.4 V and 15 pA. The UV photons were generated by a 254 nm Hg lamp and introduced into the UHV chamber through a quartz view port (transmittance greater than 90% between 200 to 800 nm) with an incident angle of 20° to the sample surface with the sample held at 15K. A lens is used to concentrate the photons to a surface spot with a diameter of approximately 4 mm. The increased temperature (15K) during UV irradiation is attributed to opening a port on the STMcryogenic shroud during the irradiation period.

III. Computational Methods.

Computations were performed with periodic density functional theory (DFT) using Vienna Abinitio Simulation Package (VASP)^{29,30} version 5.4.4. or with the program Gaussian 09.³¹ The single molecule DFT calculations were performed using the B3LYP functional and the 6-

311G++(d) basis. All Gaussian calculations were made on single molecules in the gas-phase. These resulting optimized structures were used as a starting point for subsequent VASP calculations.

The VASP code uses the projector augmented wave (PAW) method^{30,32} to describe the core electrons and valence-core interactions. We primarily used SCAN + rVV10 functional of Peng and co-workers³³⁻³⁵ with PAW potentials optimized for the PBE functional³⁶ but also compared some of the energies and structures with the B86-vdW functional. Calculations using the B86-vdW functional give qualitatively similar results with the desorption energies about 10% larger. The electronic energies reported here were calculated at the Gamma point. A plane wave cut off energy of 550 eV was used for all simulations. Methfessel-Paxton smearing was used to set the partial occupancies for each wave function with a smearing width of 0.2 eV. All the geometries were fully optimized up to 0.001 eV energy and less than 0.01 eV/Angstrom forces. The choice of our DFT methodology and plane wave cutoff energies was based on previous periodic DFT simulations of systems of similar type³⁷⁻⁴¹ and size.⁴² Additional computational details are presented in the Electronic ESI. VASP Supplementary Information, calculations for species on Au were performed (1) on a supercell composed of three layers of 4x10 Au(111) with the bottom two layers frozen at the experimental crystal structure and a 1.6 nm vacuum space, (2) upon the same supercell having molecules on the above Au, and (3) upon a single S2(CH3)2 molecule (without Au) all in the same size supercell. We also estimated the dissociation activation energy by fixing the S atoms at positions along the line between the equilibrium surface structure of DMDS and that of the lowest energy pair of dissociated radicals (see Figures S2-S4).

IV. Results and Discussion.

Single-molecule investigation. Dimethyl disulfide is a polyatomic molecule consisting of two SCH₃ groups joined by a disulfide bridge. This simple polyatomic species allows for microscopic investigation of conformational changes by examining the dissociative behavior using electrons created by tip-pulses^{27,28} or photon irradiation.⁴³ The dissociative behavior of DMDS is used to address and clarify the molecular structures of CH₃SSCH₃ versus two SCH₃ fragments. As shown in Figure 1, STM images of these molecular structures can be simplified to an ellipsoid for CH₃SSCH₃ and two individual paraboloids for 2SCH₃.

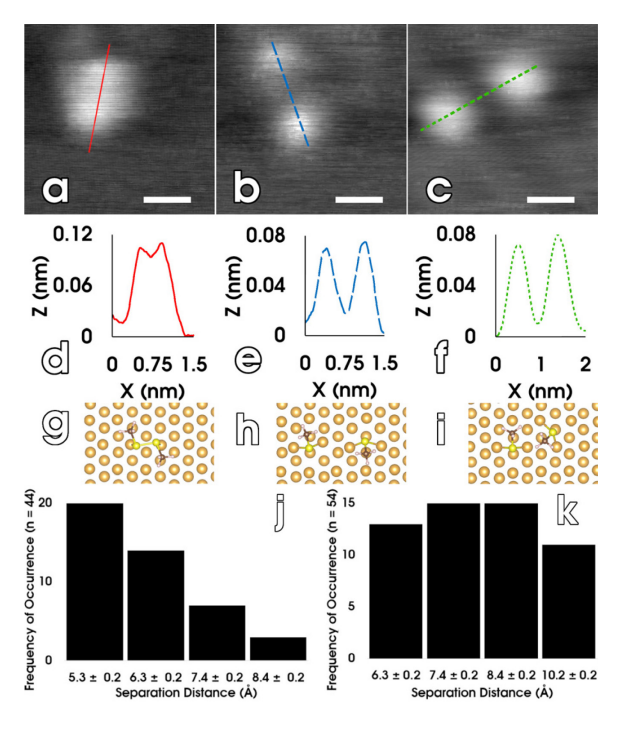


Figure 1. (a) Single-molecule DMDS deposited on Au(111) at 12K, its molecular structure is imaged as an ellipsoid with two inner lobes corresponding with the methyl groups. (b) Dissociated DMDS to 2SCH3, by tip-pulse, the molecular structure is imaged as two paraboloids. (c) Dissociated DMDS to 2SCH3 via UV (254nm) photon, imaged as two paraboloids. (d), (e), (f) Corresponding STM line-profiles of DMDS (red line) and 2SCH3 (tip-pulse dissociation (blue dash line), UV 254nm dissociation (green dotted line)) each peak represents the center of each lobe. (g) DFT optimized structure of DMDS, $E_{ads} = -1.01 \text{ eV}$. (h), (i) Projected DFT optimized structures of 2SCH3 with differing methyl group orientations; energies of adsorption for the pair of radicals relative to gas phase DMDS are: (h) $E_{ads} = -1.57 \text{ eV}$, (i) $E_{ads} = -1.36 \text{ eV}$. (j) A histogram profile of Frequency of Occurrence

versus Separation Distance for tip-induced dissociation of DMDS. (k) A histogram profile Frequency of Occurrence versus Separation Distance for UV dissociation of DMDS. The white scale bar for (a), (b), (c) is 5 Å.

The STM image of Figure 1a reveals the molecular structure of DMDS as an ellipsoid with two inner lobes, with each lobe representing the two methyl groups of similar apparent height. A line profile measurement was made on multiple molecules, and we report an average length (from edge-to-edge) of 7.0 ± 0.2 Å which is consistent to earlier published values of DMDS adsorbed on Cu (111) surface.⁴⁴

The mechanism on tip-induced dissociation of the S-S bond cleavage in DMDS molecules deposited on Cu (111) have been previously reported as an indirect vibrational mechanism^{43,45} and on Au (111) surfaces to be a direct electronic excitation mechanism.^{27,28} The activation of the specific mechanism is determined by the threshold energy generated by the tip-pulse. On Cu the report dissociation occurs below 0.4V tip bias. In contrast, the study by Maksymovych and co-workers on Au(111) reported that tip-induced direct dissociate of DMDS on Au(111) at 5K only occurred at voltages of 1.4 V or greater. Thus, they assigned the dissociation to a direct electronic process. ²⁷ They reported a S to S separation distance measuring 5.5 Å (equivalent to two lattice constants).²⁷ Our study of tip-induced dissociation of DMDS on Au(111) at 12K with a tip-pulse energy of 1.4 V showed identical results; that is, a single ellipsoid separating into two paraboloids as shown in Figure 1b. The two lobes had similar height profile relative to each other. Furthermore, Figure 1j is a histogram on the Frequency of Occurrence versus Separation Distance for tip-induced dissociation. The histogram reveals that a majority of the fragments had a separation distance measuring 5.3 ± 0.2 Å and 6.3 ± 0.2 Å. Additionally, dissociated fragments with a separation ≥ 7.4 0.2 Å indicates that the SCH₃ fragments have hopped to a different adsorption site. These hopping scenarios occurred ~23% of the total events and agrees well with the findings made by Peter and co-workers.²⁷ We never observed dissociation at 0.7 V or below, clearly supporting the direct electronic excitation (on Au) assigned by Maksymovych.

The STM image in Figure 1c shows two SCH₃ dissociated fragments after 254 nm UV photon irradiation of DMDS on Au(111) at 15K. The molecular structure shows two paraboloid structures being consistent with literature. 43,46 The histogram in Figure 1k shows Frequency of Occurrence versus Separation Distance for several UV dissociation events with separation distances ranging from 6.3 ± 0.2 Å to 10.2 ± 0.2 Å. UV dissociation results in multiple SCH3 frament separation distances and a nearly flat distribution between 6 and 10 nm. Note that the shortest separation distance (5.3 \pm 0.2 Å) after UV irradiation is not observed. These larger, evenly distributed, separation distances suggest that the dissociated fragments have hopped to neighboring adsorption sites and the S-S bond cleavage is governed by a different mechanism than that of the tip induced fragmentation. Earlier reports on gas phase DMDS photo dissociation revealed that the S-S bond is cleaved through an excited electronic state.⁴ Specifically, Schnorr and co-workers reported photo dissociation of DMDS with 267nm photons to excite the nonbonding sulfur electron to the antibonding σ_{SS}^* orbital for S-S bond cleavage.47 However, for molecules adsorbed onto a low-temperature surface additional mechanisms have been proposed, such as indirect substrate-mediate (hot electrons) excitation along with electronic excitations.43 Due to the nature of the experimental setup, the Au(111) substrate is also irradiated and generation of hot (secondary) electrons for dissociation is possible.

In addition, our utilization of a Hg, 254nm (4.9) eV) lamp for photo dissociation, the emitted photon contains much greater energy than the electron produced by the tip-pulse (1.4 eV) in our tip-induced dissociation experiments. It is likely that we are exciting a higher electronic state with the photons than with electrons. This will result in SCH₃ fragments having greater kinetic energy which can overcome the kinetic barrier necessary to hop to other adsorption sites resulting in greater separation distances. We should mention that Kazume and coworkers saw photo-induced dissociation of DMDS on Ag(111) and on Cu(111) using much lower energy visible light.43 It is likely that the electronic state in those cases lies below the one we are exciting.

To understand the final separation distance, we combined our STM images with optimized adsorption structures of CH₃SSCH₃ and two SCH₃ groups from various initial configurations. For the single-molecule DMDS-Au(111) system, we took advantage of our knowledge about the Au 4×10×3 supercell described above. Figure 1g, 1h, and 1i, are the optimized configurations for CH₃SSCH₃, that places each S atom near the top of a Au atom. For the structures of the dissociated SCH3 fragments, the S atoms are placed at a bridge site with a small shift towards the fcc (hcp)-hollow site. These structures are consistent with previous studies. 48,49 Our calculations shows the adsorption energies of 2SCH₃ relative to gas phase DMDS to be: (1) -1.56 eV with a methyl-to-methyl separation of 6.3 Å (Figure 1h) and (2) -1.36 eV with a shorter methyl distance at 3.5 Å (Figure 1i). Several other possible configurations of the SCH₃ fragments are observed experimentally and a selection of them and desorption energies (to DMDS) are presented in the S.I. Figure S4. The distribution of the tip induced radicals is cooperative in the sense that they energetically favor the structure where the fragments retain the trans orientation of the DMDS and are separated as little as possible.

The small differences in adsorption energy for the various SCH₃ fragment positions combined with our STM results imply that there is a range of possible orientations of the 2SCH₃ products.

In the dissociation reaction $CH_3SSCH_3 \rightarrow 2SCH_3$ taking place on the surface, either by tip-induced electrons or UV photon irradiation the qualitative structure changes were similar in all events, showing a single ellipsoid separating into two paraboloids with the two S atoms having a separation distance being greater or equal to two lattice constants. The significantly larger values of the product separation observed by the UV dissociation suggest that UV-induced cleavage of DMDS provides sufficient kinetic energy to the fragments to allow them to cross the barrier to diffusion several times before equilibrating with the cold surface.

CH₃SSCH₃ deposition at low temperatures: a cold-synthesis approach. Figure 2a and 2b, show a Au(111) surface exposed to a low concentration of DMDS gas beam at 12K. The adsorbed molecules show a fairly random surface distribution with no discernable order, and the appearance of each molecule as an ellipsoid indicating no dissociation has occurred. On closer observation, DMDS adsorbs with six equivalent adsorption orientations due to its two isomers being adsorbed on the 3-fold symmetric Au(111) reconstructed surface. These geometric orientations have also been reported by Ohara and co-workers on a Cu (111) surface.44 Following deposition, the sample was annealed to study the interaction of DMDS with the 22 × V3 herringbone reconstructed Au(111) surface. Figure 2 show a series of STM images after the sample was annealed to 80K. In each image, the randomness in surface morphology disappeared and a new stripe pattern emerges. The reorganization of DMDS molecules on the surface appears to be affected by the herringbone reconstruction. According to the literature, the reconstruction induces a periodic

potential acting on the surface electrons with fcc-regions having the highest reactivity followed by the hcp-regions than the soliton lines. 50 The local variation in the Au(111) reconstructed surface can be explained by electrons of the hcp-regions being less strongly bound by a potential of 15 ± 5 meV and with fcc-regions even less by 37 ± 5 meV compared to the soliton lines. 50 This periodic surface potential creates the preferential adsorption region.

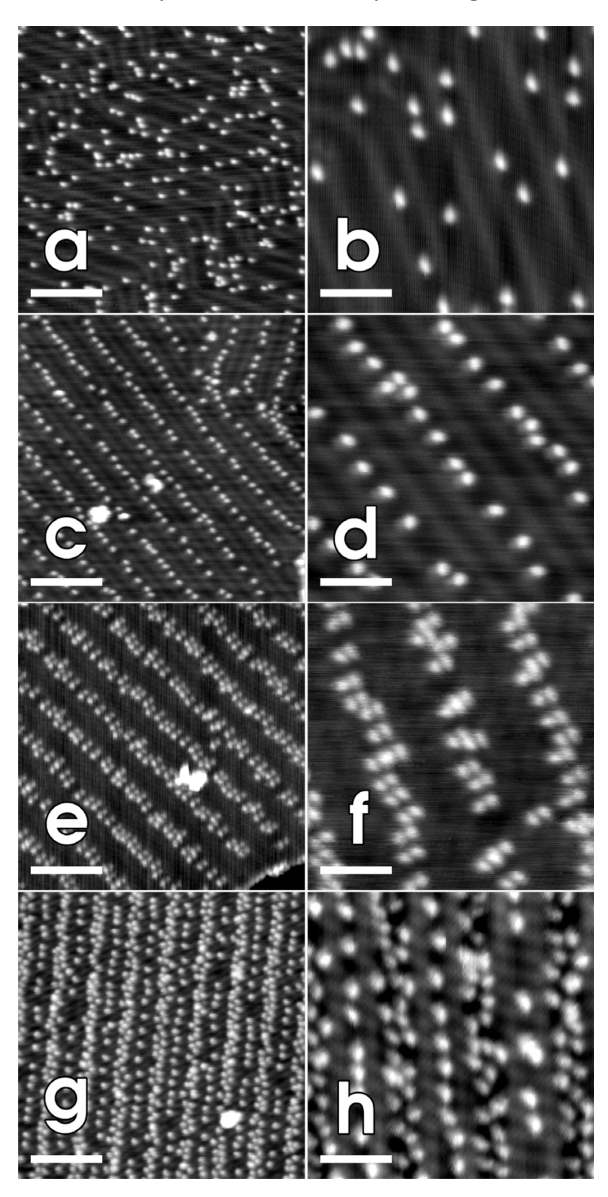


Figure 2. Low surface coverage of DMDS deposited on a Au(111) reconstructed surface at 12K. (a), (b) Surface morphology before annealing. (c), (d); (e), (f); (g), (h) Surface morphology after annealing to 80K. Each set are

samples with increasing initial surface coverage. Regular patterns can be seen on the surface. Each set of images represent a different pattern: (c, d) single-file; (e, f) double-file; (g, h) single-file and staggered (SFS). The white scale bar for (a), (c), (e), (g) is 125 Å. The white scale bar for (b), (d), (f), (h) is 50 Å.

To demonstrate preferential adsorption of **DMDS** induced by the herringbone reconstruction, we adjusted the initial surface coverage at increasing concentration intervals with subsequent annealing to 80K. Figure 2c and 2d, reveal the evolution of a stripe phase where individual DMDS molecules form a single-file columns on top of the fcc-regions. The columns of molecules are parallel with the $\langle 11\overline{2} \rangle$ crystallographic direction with a column-tocolumn distance measuring 64 ± 1.4 Å that matches the reconstruction line spacing of a clean Au(111) reconstructed surface. This observation suggests that the substrate remains unaltered with intermediate molecule-substrate interactions. Figure 2e and 2f, show annealed samples of higher initial surface concentration. Instead of single-file columns, two DMDS molecules can be seen next-to-each-other forming a double-file column in each fcc-domain. The molecule-to-molecule distance is measured to be an average spacing of 8.6 ± 0.3 Å with a column spacing of 64 ± 1.2 Å. The STM image shows local ordering of the molecule being consistent between the fcc-regions, which also suggest an intermediate molecule-substrate interaction. At greater surface concentration shown in Figure 2g and 2h, we begin to see a crossover of DMDS molecules adsorbing onto the hcp-regions. From the images, a new surface geometry evolves with DMDS column adsorbed on both the hcp and fcc-regions. In this new geometry which we will refer to as, single-file and staggered (SFS) the molecules in the fccregions are not paired next-to-each-other and transitioned to a staggered pattern. Based on the STM image the following can be observed: (1) a large portion of the molecules are staggered with a much greater molecule-tomolecule distance averaging $\geq 10 \pm 0.4 \text{ Å}$, and (2) some DMDS molecules appear in pairs with an average distance of 5.5 ± 0.2 Å. The evolution between the phases of Figure 2f to 2h, suggests that the fcc-region is able to accommodate DMDS molecules until the molecules in the double-file regime transition into the staggered regime. For the SFS morphology we can therefore draw the following conclusion: (1) as the fcc-region is loaded with more DMDS molecules there is a reduction in the local potential; (2) once the local potential of the hcpregion is greater than the fcc-region, adsorption onto the hcp-region begins; and (3) and there is an increased contribution from intermolecular interactions along with a decreased contribution from molecule-substrate interaction. Finally, for all annealed samples at low surface coverage, no adsorption onto the soliton lines are observed. These images thus represent preferential adsorption of DMDS molecules onto each specific region of the Au(111) reconstructed surface.

So far, the deposition of DMDS on the Au(111) surface has been conducted at low temperatures with low surface coverage. 43,44 We have shown that the region with highest reactivity is the fccregion followed by the hcp-region with no adsorption onto the soliton lines. In contrast, preferential adsorption was not observed on a Cu (111) surface. Furthermore, Figure 2 show additional contribution from molecule-molecule interactions with increasing surface concentration. To further understand the adsorption behavior of the DMDS-Au(111) system, we transitioned to a saturated coverage regime to investigate if the preferential adsorption behavior persists.

Figure 3, reveals the evolution of a DMDS selfassembled monolayer (SAM) on the Au(111) reconstructed surface after a sample at saturation coverage is annealed to 80K. In Figure 3a, no discernible features can be observed

associated with the DMDS molecule. The image represents a highly saturated Au(111) surface, which suggests an amorphous multilayer of DMDS molecules. While the STM image of the underlying Au(111) substrate cannot be seen, deformation to the reconstructed surface can be ruled out. As we have previously shown that DMDS deposited at low-temperatures does not dissociate upon adsorption, the possibility of forming a S-Au chemical bond is therefore low. If dissociation were to occur, that is $CH_3SSCH_3 \rightarrow$ 2SCH₃, the product would be similar to the adsorption of shortest-chain alkanethiolates, SCH₃ on the surface. As known from the literature, room-temperature saturation coverage of alkanethiols on the Au(111) substrate leads to self-assembly. 51-53 The details of that self-assembly process are well understood⁵⁴ to include a loss of the reconstruction lines, formation of domain boundaries and gold vacancy pits due to a lateral shift in Au surface atoms. These physical changes are not observed in Figure 3a.

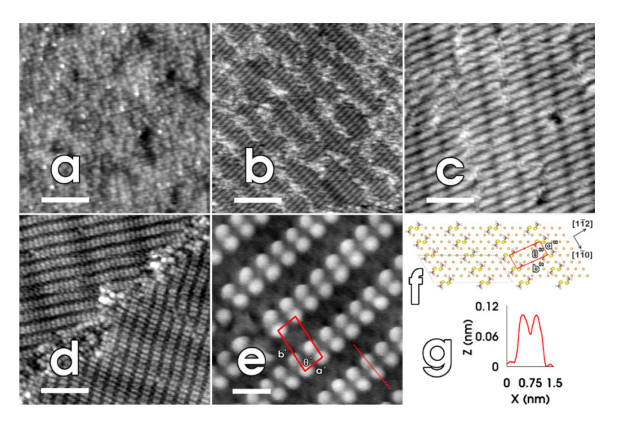


Figure 3. (a) Saturation coverage of a Au(111) surface with DMDS molecules, before annealing. (b) A large-scale STM image of a saturated sample annealed to 80K revealing amorphous DMDS intercalated within the monolayer. (c) Further annealing at 80K reveals a complete SAM. (d) A STM image of a DMDS SAM with a domain boundary at the 120° elbow of a reconstruction line (running across the diagonal from top-right corner to bottom-left corner). (e) A high-resolution image of the DMDS monolayer, each individual DMDS molecule can be seen stacked side-by-side (major axis) forming individual rows. The unit cell (in red) is overlaid on top of the image with vectors $a'' = 5.40 \pm 0.5 \, \mathring{A}$, $b' = 12.7 \pm 0.5 \, \mathring{A}$, and angle $\theta' = 79.9 \pm 5^\circ$. (f) A DFT optimized DMDS SAM and unit cell (in red) with vectors $a'' = 5.80 \, \mathring{A}$, $b'' = 12.6 \, \mathring{A}$

Å, and angle $\Theta'' = 84.0^{\circ}$. (g) Corresponding line profile (red line on (e)) of a single DMDS molecule. The white scale bar in each image: (a), (d) is 50 Å; (b), (c) is 125 Å; (e) is 10 Å.

Figure 3 follows the formation of a DMDS SAM on the Au(111) reconstructed surface by thermally induced desorption. Our results differ from previous work by Maksymovych and coworkers in studying DMDS-chain formation,⁵⁵ in that we discontinue annealing as soon as a full monolayer is formed.

The STM images seen in Figure 3d and 3e reveal a full coverage SAM formed on the Au(111) surface. After a period of annealing, excess molecules from the overlayer have desorbed to form a single layer of molecules. Figure 3b shows multiple areas of amorphous DMDS molecules intercalated with the ordered monolayer. Further annealing is observed to lead to a surface morphology shown in Figure 3c, where the overlayer is predominately comprised of a long-range single-domain DMDS monolayer.

Figure 3c, shows that in contrast to the case of the stripe phases at low surface coverage the strength of the molecule-molecule interactions in the SAM are greater than the local interaction between DMDS and the Au(111) reconstructed surface. One evidence is the adsorption of DMDS molecules onto the soliton lines. Other physical properties of the SAM, such as organizing into large single-domains (Figure 3c), suggest that the strong lateral interactions between molecules are important for the stability of the monolayer. By analyzing the underlying Au(111) substrate, one finds that the herringbone reconstruction features remain unaltered. In Figure 3d, the unaltered reconstructed surface modulates the SAM, that is, the singular monolayer domains orient in unison with the $\langle 112 \rangle$ crystallographic direction with a domain boundary forming at the 120° elbows. With a closer investigation of the SAM in Figure 3e, molecules are paired next-toeach-other to form a stacked row along the $\langle 1\bar{1}0 \rangle$ crystallographic direction with a ~5 Å gap

between each row. This self-assembly morphology appears similar to the noncovalently bound dialkyl disulfides on highly oriented pyrolytic graphite (HOPG) with the molecules adopting a tail-to-tail morphology.¹⁶ This process was reported to involve the disulfide bridge being intact and each dialkyl disulfide pair next-to-each-other along its major axis forming stacked rows. Within a single domain, a gap is present between each row as tail-to-tail adsorption orientation experiences vdW repulsion that separates each long-range row of dialkyl disulfide. In order to gain insight into the origin of the widely spaced rows of the DMDS monolayer, we computed the average desorption energy per molecule of the monolayer (0.93 eV) and found it to be significantly less than for an individual molecule at about 0.25 coverage (-1.01 eV). Thus, there is significant repulsive interaction between the adsorbed molecules. Apparently, the best balance between overall adsorption energy and intermolecular repulsion occurs at the observed row separation. The CONTCAR structure file for the optimized monolayer is provided in the SI.

Comparing the molecules of the monolayer to the single-molecule DMDS, the STM images reveal an ellipsoid structure for each molecule from the SAM. Figure 3g contains a line profile across a single DMDS molecule (from the SAM) with a lobe-to-lobe distance averaging 3.5 ± 0.2 A and the overall length (edge-to-edge) of each molecule averaging 7.0 ± 0.2 Å. These values are consistent with the single-molecule measurements from Figure 1. Based on our single-molecule and dissociation analysis (Figure 1), the monolayer shown in Figure 3 is formed by non-dissociated DMDS molecules. Structural analysis of the monolayer reveals an oblique unit structure that is commensurate with one molecule per unit cell with lattice values measuring: $a' = 5.40 \pm 0.5 \text{ Å}$, $b' = 12.7 \pm 0.5 \text{ Å}$, and $\Theta' = 79.9 \pm 5^{\circ}$. These experimental values are in good agreement with the projected DFT

optimized SAM and unit cell: a" = 5.80 Å, b" = 12.6 Å Θ " = 84.0° (Figure 3f). Furthermore, we are able to assign the a-vector to be parallel with the $\langle 1\bar{1}0 \rangle$ crystallographic direction with the b-vector angled at 12 ± 1° away from the $\langle 11\bar{2} \rangle$ crystallographic direction (the Au(111) reconstruction line). Overall, the STM results combined with the projected DFT model suggests the monolayer forms epitaxially with the Au(111) surface and is not constrained by the soliton lines as seen with the low surface coverage regime of Figure 2.

CH₃SSCH₃ deposition at elevated temperatures (80K & 120K): a hot-synthesis approach. Previous reports of HREELS for DMDS adsorption on Au(111) suggest that DMDS molecules adsorb without dissociation at temperatures less than 150K. 50 Based on that report, one would predict identical surface morphologies for deposition at any temperature below 150K. Figure 4a, 4b and 4c, 4d; are sets of STM images of the Au(111) reconstructed surface exposed to a low dose of DMDS gas at 80K and 120K. The formation of stripe phases on the surface is observed. Initially it might appear that these surfaces are similar to the DMDS-Au(111) system that was formed by depositing DMDS at low temperatures followed by annealing to the respective temperatures (see Figure 2 and S.I. Figure S1). Upon closer investigation, however, one also observes the coexistence of the dissociated SCH₃ fragments and native intact CH₃SSCH₃ on the same Au(111) surface. Figure 4b and 4d reveal both the ellipsoid and two paraboloid molecular structures corresponding to DMDS and 2SCH₃, respectively. This is most easily seen in the insets line profiles of the molecular species showing similar dimensions to the single-molecule chemical species shown in Figure 1. Thus, the nature of the surface species depends strongly on whether the deposition first occurred at 80K and was then cooled to 12K (hot synthesis) or the deposition occurred at 12K and was annealed at 80K (cold synthesis). It is well known that kinetic processes can compete and even dominate over thermodynamic equilibrium when forming self-assembled monolayers. ⁵⁶ Clearly, at least one of these structures cannot be at thermal equilibrium.

Since our DFT calculated values for E_{ads} (Figure 1) indicate that the dissociated species is thermodynamically more stable, the issue is one of kinetics rather than thermodynamics. We have computed the electronic energy of the DMDS as it progressively dissociates into the energy optimal configuration of 2SCH₃ species in terms of linear increase in S-S distance from Figure 1g to 1i, and find that the barrier is about 0.5 eV (see SI). Jaccob and co-workers ⁵⁷ used very different computation methods and found a dissociation barrier height on Au(111) to be 0.75 eV. Thus, both computational and experimental results indicate that a kinetic barrier traps DMDS during low temperature deposition.

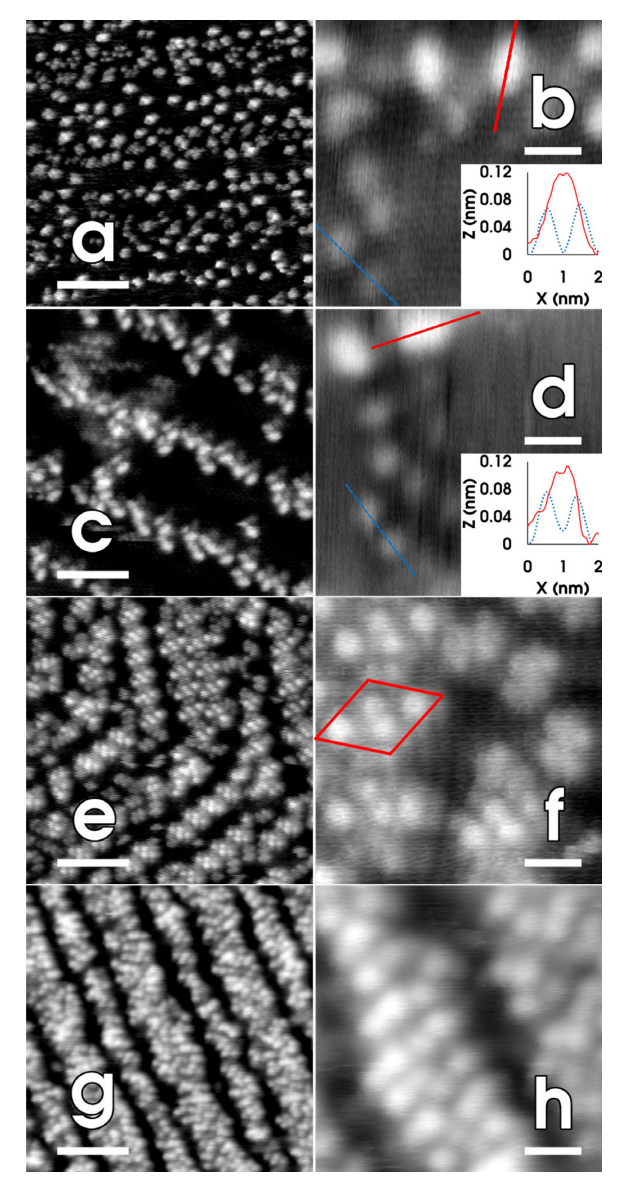


Figure 4. (a), (b); (c), (d) Low surface coverage of DMDS deposited at 80K (a), (b) and 120K (c), (d). The insets of (b) and (d) are line profiles taken across the major axis of each molecular species, the red line correspond to DMDS and the blue dashed line for 2SCH₃. (e), (f); (g), (h) Saturation coverage of DMDS deposited at 80K (e), (f) and 120K (g), (h). The white scale bar of (a), (c), (e), (g) is 125 Å. The white scale bar of (b), (d), (f), (h) is 10 Å.

The transition from a low surface coverage to saturated coverage at elevated deposition temperatures reveals a different surface morphology than seen in the cold synthesis. The coexistence of both DMDS and SCH₃ fragments precludes the formation of a DMDS SAM at saturated coverages, and no ordered monolayer

is observed on the surface at 80K or 120K deposition temperatures, as shown in Figure 4e and 4g, respectively. Instead of an ordered SAM, saturated column of molecules can be observed on the entire surface. The adlayer shown in Figure 4f shows some local ordering in its structure (red diamond), while Figure 4h appears to have a random morphology in each column. At these elevated deposition temperatures and concentrations, the herringbone reconstruction appears to have remained intact as we can clearly see a separation between each column of molecules. The separation between the columns suggests that there are local variations present on the surface with the least favorable adsorption region (soliton lines) still in place and acting as a barrier with only the fcc and hcp regions interacting with DMDS and SCH₃ fragments.

V. Conclusion.

Utilizing LT-STM in UHV we have studied the DMDS-Au(111) system using different cold-synthesis versus hot-synthesis approaches. These two approaches did not converge to the same surface morphology at the same thermodynamic state. Our STM images from both approaches in conjunction with the DFT calculations show the adsorption of intact DMDS on Au(111) being governed by a kinetic barrier.

Our analysis suggests that 298K molecules impinging on a Au(111) surface at 80K or above have retained sufficient energy to occasionally dissociate. On the other hand, when impinging on the 12K surface the internal modes cool sufficiently rapidly that no dissociation occurs. Clearly the low temperature deposited system is not at thermal equilibrium, but what about the films formed by deposition at 80K and 120K. Most likely these are also kinetically trapped phases.

The surface morphologies of the DMDS-Au(111) system at low surface coverage is affected by

preferential adsorption onto different regions of the anisotropic reconstructed surface guided by molecule-substrate interactions. At high surface coverage, annealing leads to self-assembly with a balance between molecule substrate and molecule-molecule interaction that produce a SAM comprised of single-phase monolayer domains following the orientation of the reconstruction lines with domain boundaries present at the 120° elbows of the herringbone reconstruction. In contrast, to the hot-synthesis approach, neither self-assembly nor adsorption of purely intact DMDS occurs, but adsorption of both chemical species and the formation of disorder column of molecules on the surface is observed.

Another interesting feature of this study is the direct comparison of tip-induced and UV radiation induced dissociation. One finds a large difference in the spatial distributions of radical fragments formed by the two methods.

AUTHOR INFORMATION

Corresponding Author

K W Hipps - Department of Chemistry and Materials Science and Engineering Program, Washington State University, Pullman, WA 99163-4630. orcid.org/ 0000-0002-5944-5114; Email: hipps@wsu.edu.

Authors

Yi Zhang — Materials Science and Engineering Program, Washington State University, Pullman, WA 99163-4630. Orcid.org/ 0000-0003-2228-0341

Email: yi.zhang5@wsu.edu

David Y. Lee - INFICON, East Syracuse, New York 13057, United States. Orcid.org/ 0000-0002-0494-9809

Email: david.y.lee@inficon.com

SUPPORTING INFORMATION

The Supporting Information is available free of charge at XXXXX. It contains STM images of DMDS deposited on Au at 120K. It also provides VASP optimized structures for the isolated DMDS molecule and for a monolayer. Several structures and energies of CH₃ pairs on Au(111) are also provided. The CONTCAR file of the optimized SAM is also given.

Acknowledgements

Funding for this project was provided by the W.M. Keck Foundation and by the National Science Foundation under grant CHE-1807225. We gratefully acknowledge their support.

Reference

¹ Lavich, D. J.; Wetterer, S. M.; Bernasek, S. L.; Scoles, G. Physisorption and Chemisorption of Alkanethiols and Alkyl Sulfides on Au(111). *J. Phys. Chem. B* **1998**, 102, 3456-3465.

- ² Wilbur, J. L.; Folkers, J. P.; Whitesides, G. M. Differentiating Functional Groups with the Scanning Tunneling Microscope. *J. Phys. Chem.* **1995**, 99, 8684-8689.
- ³ Kelly, K. F.; Shon, Y-S.; Lee, L. R.; Halas, N. J. Scanning Tunneling Microscopy and Spectroscopy of Dialkyl Disulfide Fullerenes Inserted into Alkanethiolates SAMs. *J. Phys. Chem. B* **1999**, 103, 8639-8642.
- ⁴ Bookwalter, C. W.; Zoller, D. L.; Ross, P. L.; Johnston, M. V. Bond-Selective Photodissociation of Aliphatic Disulfides. *J. Am. Soc. Mass Spectrom* **1995,** 6, 872-876.
- ⁵ Sawaguchi, T.; Mizuani, F.; Taniguchi, I. Direct Observation of 4-Mercaptopyridine and Bis(4-pyridyl) Disulfide Monolayers on Au(111) in Perchloric Acid Solution Using In Situ Scanning Tunneling Microscopy. *Langmuir* **1998**, 14, 3565-3569.
- ⁶ Nuzzo, R. G.; Zegarski, B. R.; Dubois, L. H. Fundamental Studies of the Chemisorption of Organosulfur Compounds on Au(111). Implications for Molecular Self-Assembly on Gold Surfaces. *J. Am. Chem. Soc.* **1987**, 109, 733-739.
- ⁷ Wan, L-J.; Hara, Y.; Noda, H.; Osawa, M. Dimerization of Sulfur Headgroups in 4-Mercaptopyridine Self-Assembled Monolayers on Au(111) Studied by Scanning Tunneling Microscopy. *J. Phys. Chem. B* **1998**, 102, 5943-5946.
- ⁸ Kondoh, H.; Kodama, C.; Sumida, H.; Nozoye, H. Molecular processes of adsorption and desorption of alkanethiol monolayers on Au(111). *J. Chem. Phys.* **1999,** 111, 1175-1184.
- ⁹ Grönbeck, H.; Curioni, A.; Andreoni, W. Thiols and Disulfides on the Au(111) Surface: The Headgroup-Gold Interaction. *J. Am. Chem. Soc.* **2000**, 122, 3839-3842.
- ¹⁰ Cyr, D. M.; Venkataraman, B.; Flynn, G. W. STM Investigations of Organic Molecules Physisorbed at the Liquid-Solid Interface. *Chem. Mater.* **1996,** 8, 1600-1615.
- ¹¹ Vericat, C.; Vela, M. E.; Benitez, G.; Carro, P.; Salvarezza, R. C. Self-assembled monolayers of thiols and dithols on gold: new challenges for a well-known system. *Chem. Soc. Rev.* **2010**, 39, 1805-1834.

¹² Wang. Y.; Hush, N. S.; Reimers, J. Formation of Gold-Methanthiyl Self-Assembled Monolayers. *J. Am. Chem. Soc.* **2007**, 129, 14532-14533.

- ¹³ Kondoh, H.; Nozoye, H. Low-Temperature Ordered Phase of Methylthiolate Monolayers on Au(111). *J. Phys. Chem. B* **1999**, 103, 2585-2588.
- ¹⁴ Claypool. C. L.; Faglioni, F.; Goddard, W. A., III.; Gary, H. B.; Lewis, N. S.; Marcus, R. A. Source of Image Contrast in STM Images of Functionalized Alkanes on Graphite: A Systematic Functional Group Approach. *J. Phys. Chem. B* **1997**, 101, 5978-5995.
- ¹⁵ Guo, Q.; Li, F. Self-assembled alkanethiol monolayers on gold surfaces: resolving the complex structure at the interface by STM. *Phys. Chem. Chem. Phys.* **2014**, 16, 19074-19090.
- ¹⁶ Noh, J.; Murase, T.; Nakajima, K.; Lee, H.; Hara, M. Nanoscopic Investigation of the Self-Assembly Processes of Dialkyl Disulfides and Dialkyl sulfides on Au(111). *J. Phys. Chem. B* **2000**, 104, 7411-7416.
- ¹⁷ Bürgi, T. Properties of the gold-sulphur interface: from self-assembled monolayers to clusters. *Nanoscale* **2015**, 7, 15553-15567.
- ¹⁸ Maksymovych, P.; Dougherty, D. B. Molecular self-assembly guided by surface reconstruction: CH₃SH monolayer on the Au(111) surface. *Surface Science* **2008**, 602, 2017-2024.
- ¹⁹ Giancarlo, L. C.; Fang, H.; Rubin, S. M.; Bront, A. A.; Flynn, G. W. Influence of the Substrate on Order and Image Contrast for Physisorbed Self-Assembled Molecular Monolayers: STM Studies of Functionalized Hydrocarbons on Graphite and MoS₂. *J. Phys. Chem. B* **1998**, 102, 10255-10263.
- ²⁰ Nenchev, G.; Diaconescu, B.; Hagelberg, F.; Pohl, K. Self-assembly of methanthiol on the reconstructed Au(111) surface. *Phys. Rev. B* **2009**, 80, 081401R.
- ²¹ Hanke, F.; Björk, J. Structure and local reactivity of the Au(111) surface reconstruction. *Phys. Rev. B* **2013,** 87, 235422.
- ²² Narasimhan, S.; Vanderbilt, D. Elastic Stress Domains and the Herringbone Reconstruction on Au(111). *Phys. Rev. Lett.* **1992,** 69, 1564-1567.
- ²³ Cho, J.; Levy, N.; Kirakosian, A.; Comstock, M. J.; Lauterwasser, F.; Fréchet, J. M. J.; Crommie, M. F. Surface anchoring and dynamics of thiolated azobenzene molecules on Au(111). *J. Chem. Phys.* **2009**, 131, 034707.

²⁴ Néel, N.; Kröger, J.; Berndt, R. Fullerene nanowires on a vicinal gold surface. *Appl. Phys. Lett.* **88**, 1163101.

- ²⁵ Bohringer, M.; Morgenstern, K.; Schneider, W. D.; Berndt, R.; Mauri, F.; De Vita, A.; Car, R. Two-dimensional self-assembly of supramolecular clusters and chains. *Phys. Rev. Lett.* **1999**, 83, 324-327.
- ²⁶ Renzi, V. D.; Rousseau, R.; Marchetto, D. Biagi, R.; Scandolo, S.; Pennino, UD. Metal Work-Function Changes induced by Organic Adsorbates: A Combined Experimental and Theoretical Study. *Phys. Rev. Lett.* **2005**, 95, 046804.
- ²⁷ Maksymovych, P.; Yates, J. T., Jr. Propagation of Conformation in the Surface-Aligned Dissociation of Single CH₃SSCH₃ Molecules on Au(111). *J. Am. Chem. Soc.* **2006**, 128, 10642-10643.
- ²⁸ Maksymovych, P.; Sorescu, D. C.; Yates, J. T., Jr. Gold-Adatom-Mediated Bonding in Self-Assembled Short-Chain Alkanethiolate Species on the Au(111) Surface. *Phys. Rev. Lett.* **2006**, 97, 146103.
- ²⁹ Kresse, G.; Furthmüller, J. Efficiency of Ab-Initio Total Energy Calculations for Metals and Semiconductors Using a Plane-Wave Basis Set. *Comput. Mater. Sci.* **1996**, *6*, 15–50.
- ³⁰ Kresse, D.; Joubert, D. From Ultrasoft Pseudopotentials to the Projector Augmented-Wave Method, *Phys. Rev. B: Condens. Matter Mater. Phys.* **1999**, *59*, 1758–1775.
- ³¹ Frisch, M. J.; Trucks, G. W.; Schlegel, H. B.; Scuseria, G. E.; Robb, M. A.; Cheeseman, J. R.; Scalmani, G.; Barone, V.; Mennucci, B.; Petersson, G. A., et al. *Gaussian 09*, Revision D.01, Gaussian, Inc.: Wallingford CT, 2013.
- ³² Blöchl, P. E. Projector Augmented-Wave Method. *Phys. Rev. B* **1994**, *50*, 17953–17979.
- ³³ Klime, J.; Bowler, D. R.; Michaelides, A. Van der Waals Density Functionals Applied to Solids, *Phys. Rev. B: Condens. Matter Mater. Phys.* **2011**, *83*, 195131.
- ³⁴ Sun, J.; Ruzsinszky, A.; Perdew, J. Strongly Constrained and Appropriately Normed Semilocal Density Functional. *Phys. Rev. Let.* **2015**, 115 (036402) 5 pp.
- ³⁵ Peng, H.; Yang, Z.-H.; Perdew, J. P.; Sun, J. Versatile van der Waals Density Functional Based on a Meta-Generalized Gradient Approximation. *Phys. Rev. X* **2016**, *6*, 041005. 15 pp.
- ³⁶ Perdew, J. P.; Burke, K.; Ernzerhof, M. Generalized Gradient Approximation Made Simple. *Phys. Rev. Lett.* **1996**, *77*, 3865–3868.
- ³⁷ Tierney, H.; Calderon, C.; Baber, A. E.; Sykes, E.; Wan, F. Understanding the Rotational Mechanism of a Single Molecule: STM and DFT Investigations of Dimethyl Sulfide Molecular Rotors on Au(111). *J. Phys. Chem. C* **2010**, *114*, 3152–3155.
- ³⁸ Jahanbekam, A.; Chilukuri, B.; Mazur, U.; Hipps, K. W. A Kinetically Trapped Two-Component Self Assembled Adlayer. *J. Phys. Chem. C* **2015**, *119*, 25364–25376.

³⁹ Jie, C.; Weiyu, X.; Kaihang, L.; Shengbai, Z.; Yi-Yang, S. Benchmarking PBE+D3 and SCAN+rVV10 methods using potential energy surfaces generated with MP2+ Δ CCSD(T) calculation. *Chinese Phys. B* **2020**, *29*, 013102.

- ⁴⁰ Christian, M. S.; Otero-de-la-Roza, A.; Johnson, E. Surface Adsorption from the Exchange-Hole Dipole Moment Dispersion Model. *J. Chem. Theory Comput.* **2016**, *12*, 3305–3315.
- ⁴¹ Chilukuri, B.; Mazur, U.; Hipps, K. W. Effect of Dispersion on Surface Interactions of Cobalt(II) Octaethylporphyrin Monolayer on Au(111) and HOPG(0001) Substrates: A Comparative First Principles Study. *Phys. Chem. Chem. Phys.* **2014**, *16*, 14096–14107.
- ⁴² Rana, S.; Jiang, J.; Korpany, K.; Mazur, U.; Hipps, K. W. STM Investigation of Y[C₆S-Pc]₂ and Y[C₄O-Pc]₂ Complex at the Solution/Solid Interface: Substrate Effects, Sub-molecular Resolution, and Vacancies. *J. Phys. Chem. C* **2021**, *125*, 1421–1431.
- ⁴³ Kazuma, E.; Jung, J.; Ueba, H.; Trenary, M.; Kim, Y. Direct Pathway to Molecular Photodissociation on Metal Surfaces Using Visible Light. *J. Am. Chem. Soc.* **2017**, 139, 3115-3121.
- ⁴⁴ Ohara, M.; Kim, Y.; Kawai, M. Direct Observation of conformational Isomers of (CH₃S)₂ Molecules on Cu (111). *J. App. Phys.* **2005**, 7B, 5390-5392.
- ⁴⁵ Ohara, M.; Kim, Y.; Yanagisawa, S.; Morikawa, Y.; Kawai, M. Role of Molecular Orbitals Near the Fermi Level in the Excitation of Bivrational Modes of a Single Molecule at a Scanning Tunneling Microscope Junction. *Phys. Rev. Lett.* **2008**, 100, 136104.
- ⁴⁶ Kazuma, E.; Jung, J.; Ueba, H.; Trenary, M.; Kim, Y. Real-space and real-time observation of a plasmon-induced chemical reaction of a single molecule. *Science* **2018**, 360, 521-526.
- ⁴⁷ Schnorr, K.; Bhattacherjee, A.; Oosterbaan, K. J.; Delcey, M.; Yang, Z.; Xue, T.; Attar, A.; Chatterley, A.; Head-Gordon, M.; Leone, S. R.; Gessner, O. Tracing the 267 nm-Induced Radical Formation in Dimethyl Disulfide Using Tme-Resolved X-ray Absorption Spectroscopy. *J. Phys. Chem. Lett.* **2019**, 10, 1382-1387.
- ⁴⁸ Maksymovych, P.; Sorescu, D. C.; Yates, J. T., Jr. Methanethiolate Adsorption Site on Au(111): A Combined STM/DFT Study at the Single-Molecule Level. *J. Phys. Chem. B* **2006**, 110, 21161-21167.
- ⁴⁹ Hayashi, T. Adsorption state of dimethyl disulfide on Au(111): Evidence for adsorption as thiolate at the bridge site. *J. Chem. Phys.* **2001**, 114, 7615-7621.
- ⁵⁰ Bürgi, L.; Brune, H.; Kern, K. Imaging of Electron Potential landscapes on Au(111). *Phys. Rev. Lett.* **2002**, 89, 176801.
- ⁵¹ Renzi, V. D.; Felice, R. D.; Marchetto, D.; Biagi, R.; Pennino, U. D.; Selloni, A. Ordered (3 × 4) High-Density Phase of Methylthiolate on Au(111). *J. Phys. Chem. B* **2004**, 108, 16-20.

⁵² Noh, J.; Kato, H. S.; Kawai, M.; Hara, M. Surface and Adsoprtion Structures of Dialkyl Sulfide Self-Assembled Monolayers on Au(111). *J. Phys. Chem. B* **2002**, 106, 13268-13272.

- ⁵³ Rzeźnicka, I. I.; Lee, J.; Maksymovych, P.; Yates, J. T., Jr. Nondissociative Chemisorption of Short Chain Alkanethiols on Au(111). *J. Phys. Chem. B* **2005**, 109, 15992-15996.
- ⁵⁴ Poirier, G. E.; Pylant, E. D. The Self-Assembly Mechanism of Alkanethiols on Au(111). *Science.* **1996,** 272, 2245-2248.
- ⁵⁵ Maksymovych, P.; Sorescu, D. C.; Jordan, K. D.; Yates, J. T., Jr. Collective Reactivity of Molecular Chains Self-Assembled on a Surface. *Science* **2008**, 322, 1664-1667.
- ⁵⁶ Hipps, K.W.; Mazur, U. Kinetic and Thermodynamic Control in Porphyrin and Phthalocyanine Self-Assembled Monolayers. *Langmuir* **2018**, 34, 3–17
- ⁵⁷ Jaccob, M; Rajaraman, G.; Totti, F. On the kinetics and thermodynamics of S–X (X 5 H, CH3, SCH3, COCH3, and CN) cleavage in the formation of self-assembledmonolayers of alkylthiols on Au(111). *Theor. Chem. Acc.* **2012**, *131*, 1150 11pp.